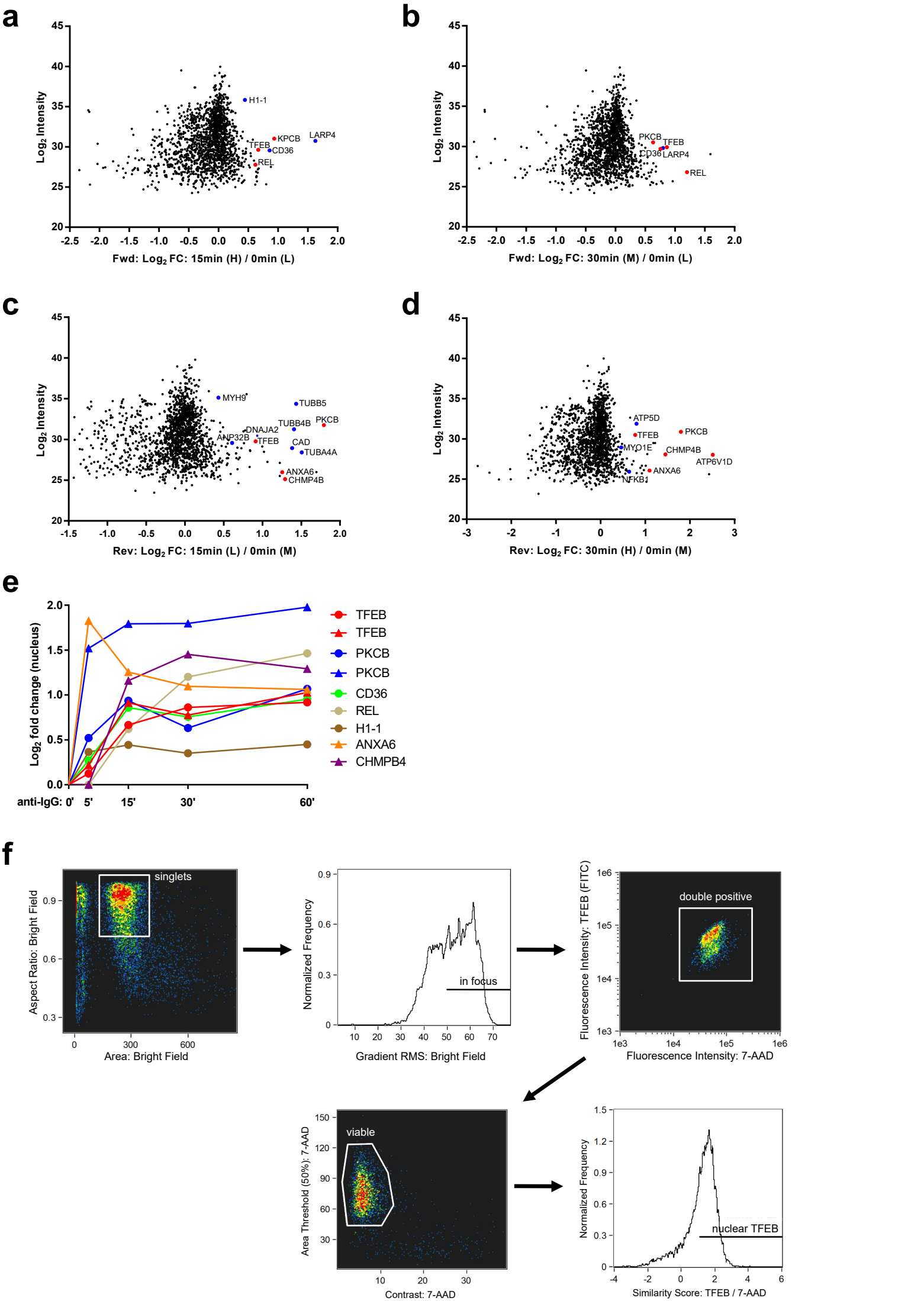

Ext. Data Fig. 1

Extended Data Fig. 1 | Proteomic replicates of the SILAC-based nuclear translocatome analysis and gating strategy of imaging flow cytometry. (a-d) Scatter plots of identified proteins in the nuclear extracts of the proteomic replicate approach **(a-b)** forward labelling (Fwd) and **(c-d)** reverse labelling (Rev) represented as the log_2-fold enrichment ('SILAC ratios') at the depicted time points, plotted against the log_2 signal intensity. Proteins significantly enriched at two timepoints are highlighted in blue, significantly enriched proteins at ≥3 time points are marked red. **(e)** Nuclear translocation kinetics of significantly enriched proteins in the proteomic replicate approach detected at all time points. Proteins detected in the forward experiment are depicted as circles, proteins identified in the reverse experiment are represented as triangles. **(f)** Gating strategy for the assessment of nuclear translocation of TFEB via imaging flow cytometry: Single cells were gated according to their size (Area) and roundness (Aspect Ratio). Focused cells were defined as having a Gradient RMS value >50. Single cells in focus were further gated according to their double-positive staining of TFEB (FITC) and the nucleus (7-AAD). Apoptotic cells were excluded using the 'apoptosis algorithm' (IDEAS software), analyzing the nuclear staining signal. Nuclear translocation of TFEB in viable cells was finally determined using the 'nuclear translocation algorithm' (IDEAS software) on the channels depicting the TFEB (FITC) and nuclear signal (7-AAD).

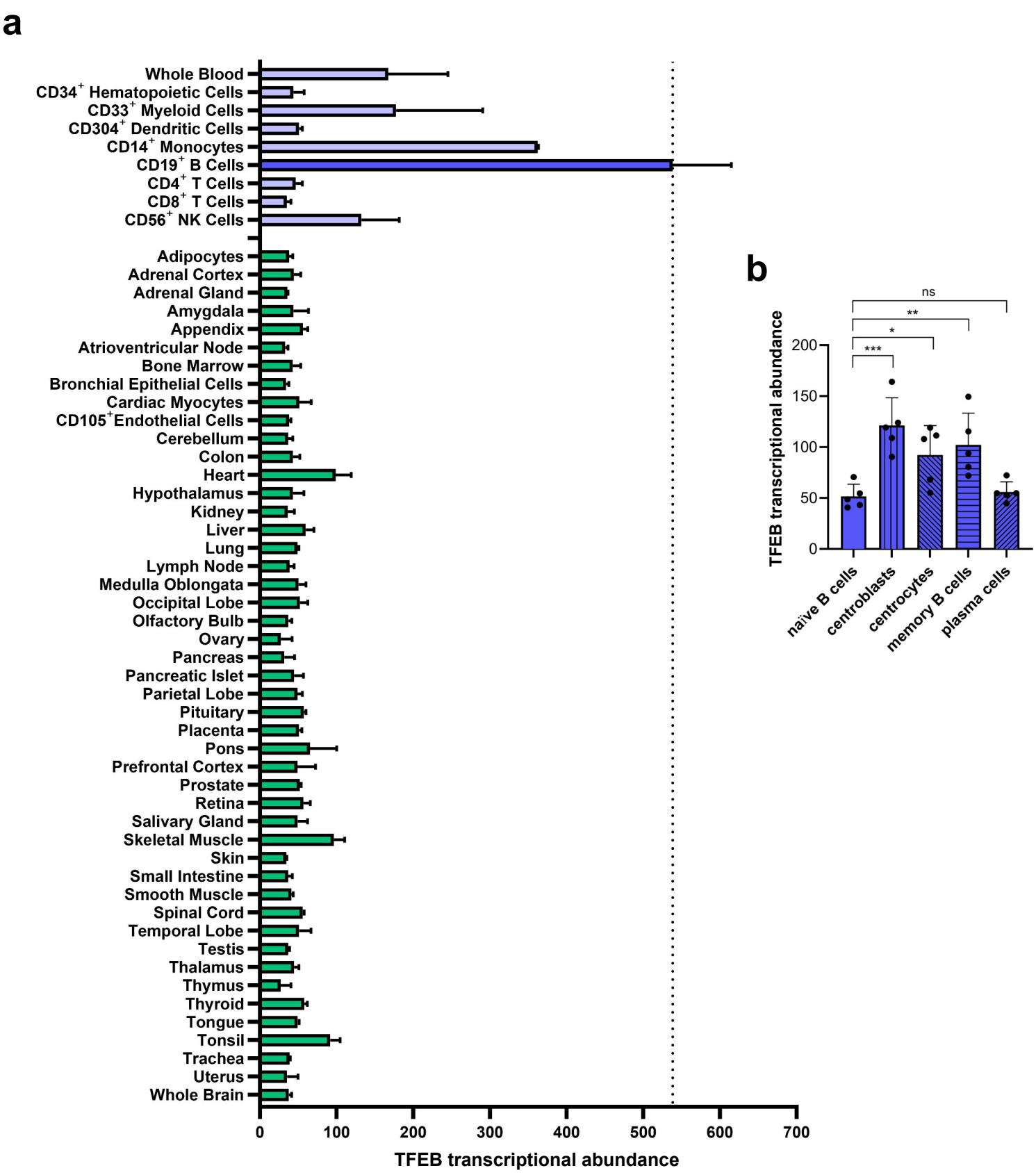

Ext. Data Fig. 2

Extended Data Fig. 2 | TFEB expression among human cell types is highest in B cells. **(a)** TFEB transcript abundance in various human tissues. This figure was derived from public microarray data (GeneAtlas U133A, 221866_at) published by Su et al, 2004 ([25]) Relative expression of TFEB in immune cells is depicted in blue, with B cells highlighted in dark blue, while TFEB expression levels in other cell types and tissues is depicted in green. **(b)** Comparison of TFEB transcription levels in major human B cells subsets with antigenic experience. Expression data was derived from public microarray data (GSE12453) published by Brune et al., 2008 ([26]). TFEB mRNA expression is depicted as mean±SD of five independent samples per subset. Significances were calculated using an unpaired, two-tailed student's t-test. ****: $p<0.0001$, ***: $p<0.001$, **: $p<0.01$, *: $p<0.05$.

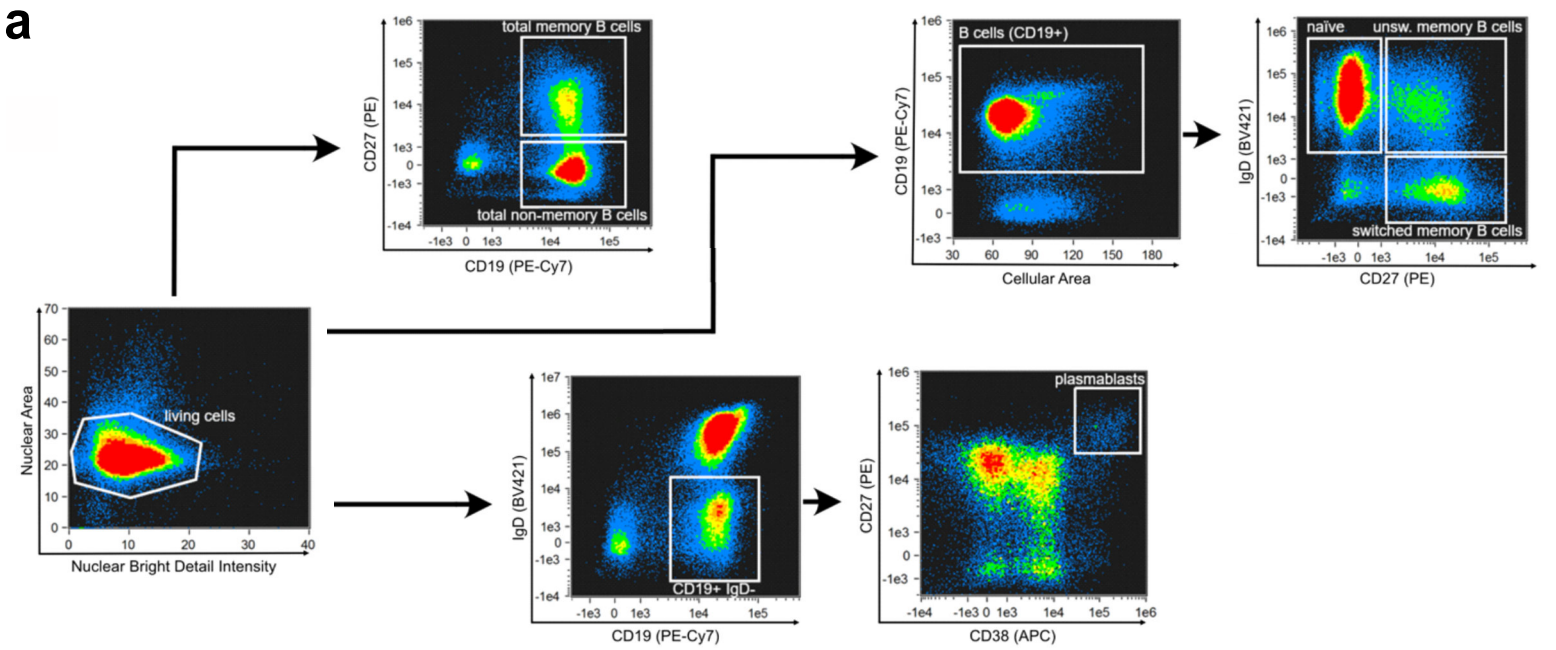

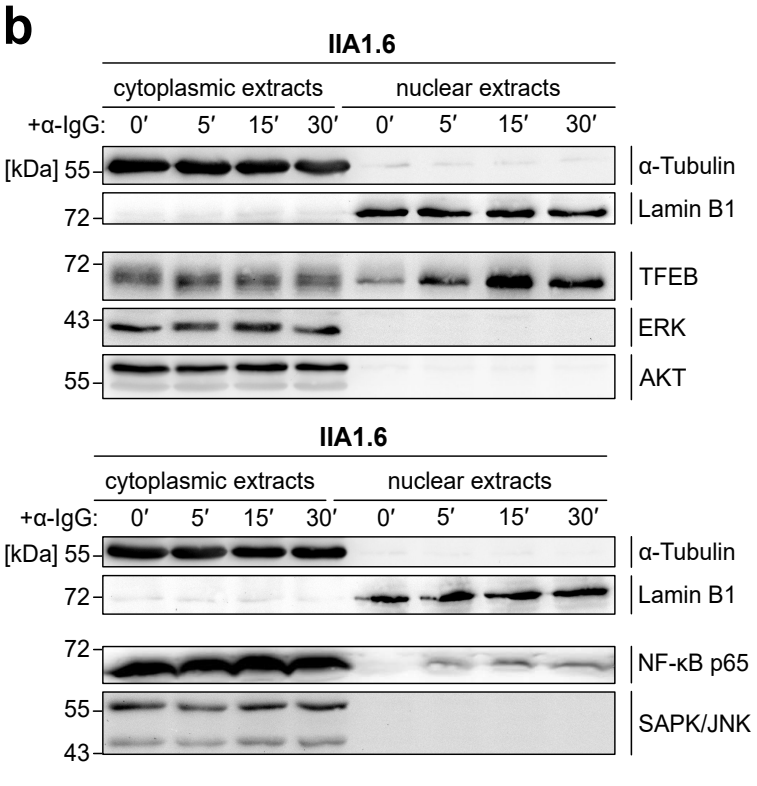

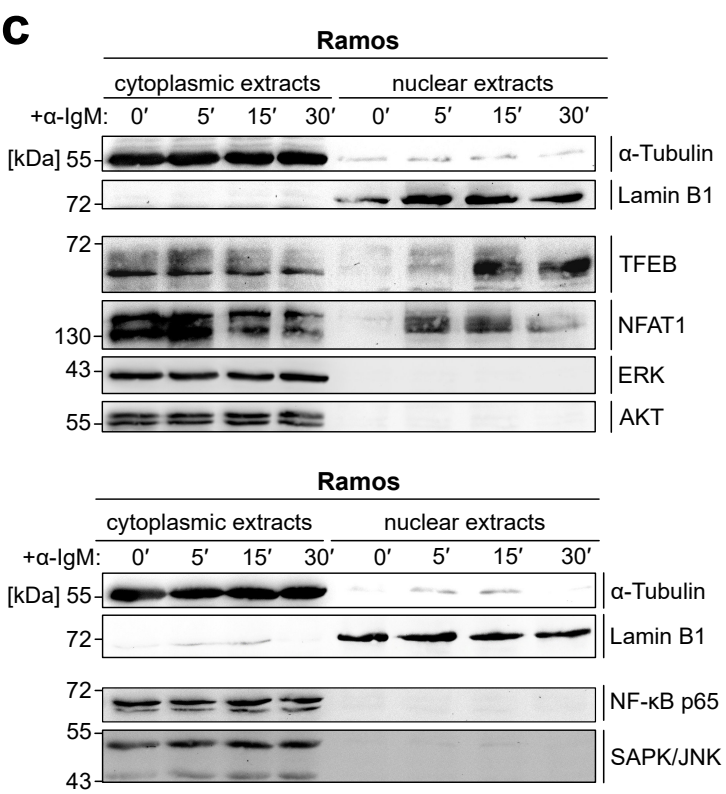

Ext. Data Fig. 3

Extended Data Fig. 3 | Flow cytometry gating of human B cells and biochemical monitoring of the nuclear translocation of various B cell effector proteins. (a) Multi-color imaging flow cytometric gating strategy of human B cell subsets: Single, focused cells were gated according to their size ('Area') and roundness ('Aspect Ratio'). Upon exclusion of apoptotic and out-of-focus cells (not shown), total non-memory B cells ($CD19^+CD27^-$), total-memory ($CD19^+CD27^+$), naïve ($CD19^+CD27^-IgD^+$), unswitched memory ($CD19^+CD27^+IgD^+$), switched memory ($CD19^+CD27^+IgD^-$) and plasmablasts ($CD19^+CD27^+IgD^-CD38^+$) were distinguished by differential expression of the surface markers CD19, CD27, CD38 and IgD as depicted in the gating scheme. **(b-c)** Resting or BCR-activated IIA1.6 or Ramos (**b** and **c**, respectively) B cells were subjected to subcellular fractionation via lysis gradient centrifugation. Cytosolic and nuclear fractions were separated by SDS-PAGE and subjected to Western Blot analysis using antibodies recognizing the signaling proteins indicated on the right. Relative molecular masses of marker proteins are indicated on the left in kDa and anti-β-actin staining was used to confirm equal protein loading.

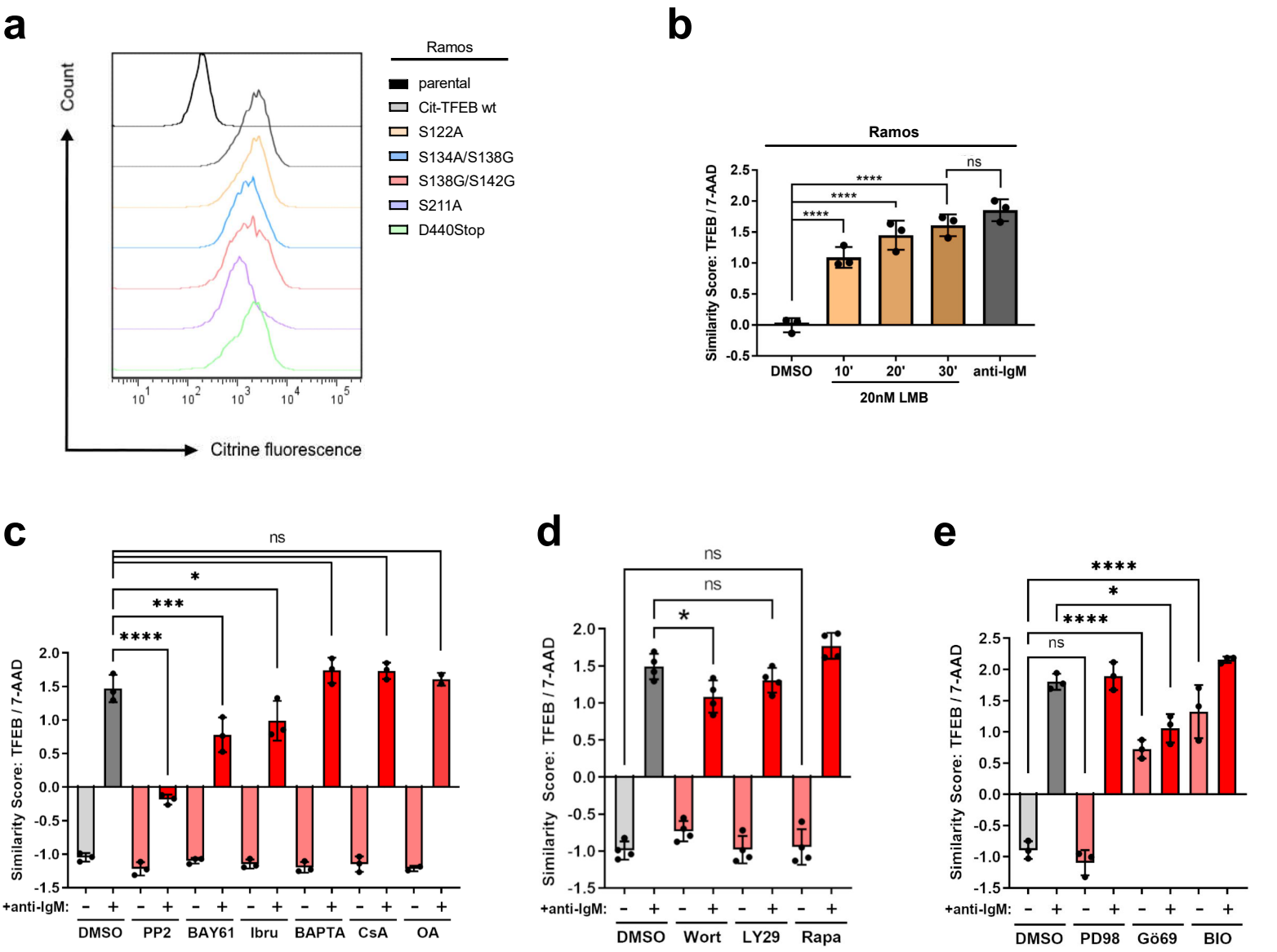

Ext. Data Fig. 4

Extended Data Fig. 4 | Assessment of the regulatory signal network underlying TFEB translocation in Ramos B cells. (a) Wild-type Ramos cells were retrovirally transduced with citrine-tagged full-length human TFEB or mutated variants of TFEB. Equal expression of the citrine-TFEB fusion protein was confirmed via flow cytometry. **(b)** Ramos B cells were left untreated (-), treated with 20 nM leptomycin B (LMB) for the indicated time periods or BCR-activated and the nuclear translocation of TFEB was monitored by imaging flow cytometry as defined by mean similarity score of TFEB/7-AAD. Data are depicted as mean±SD of three independent experiments. Statistical significances were calculated using one-way ANOVA and corrected for multiple testing via Tukey's method. ****: $p<0.0001$, ***: $p<0.001$, **: $p<0.01$, *: $p<0.05$. **(c-e)** Impact of various signaling inhibitors on the nuclear translocation of TFEB as defined by mean similarity scores of TFEB versus 7-AAD. Wild-type Ramos B cells were left untreated (-) or BCR-activated (+, 60 min) in the presence of the indicated pharmacological agents. PP2, BAY61 or ibrutinib (inhibiting Src, Syk or Btk, respectively), or the Ca^{2+} chelator BAPTA-AM, or cyclosporin A (inhibitior of calcineurin), okadaic acid (inhibitor of phosphatases PP1 and 2), wortmannin or LY294002 (both antagonizing PI3K), rapamycin (mTOR inhibitor), PD98059 (ERK inhibitor), BIO-acetoxime (GSK3β inhibitor) or Gö6983 (PKC inhibitor). Each of the inhibitors were added to the cells 15 min before BCR ligation and were controlled by treatment of the cells with 1% DMSO. Nuclear TFEB was defined by mean similarity scores of TFEB versus 7-AAD. Data are depicted as mean±SD of three independent experiments. Statistical significances were computed using one-way ANOVA and corrected for multiple testing via Tukey's method. ****: $p<0.0001$, ***: $p<0.001$, **: $p<0.01$, *: $p<0.05$.

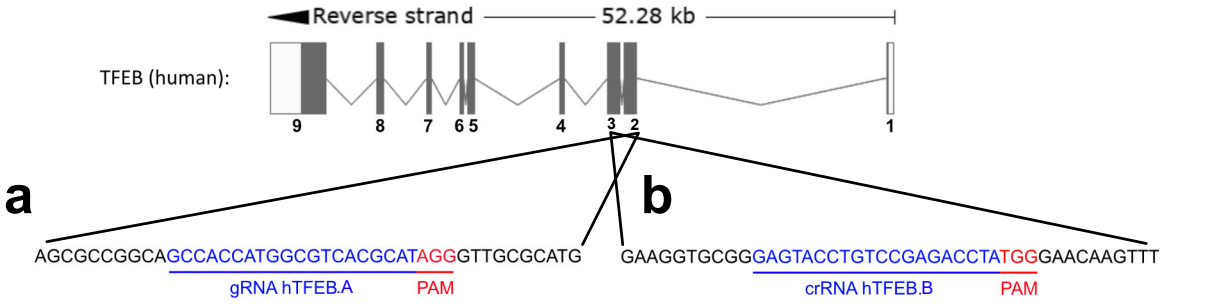

a

AGCGCCGGCAGCCACCATGGCGTCACGCATAGGGTTGCGCATG

gRNA hTFEB.A PAM

b

GAAGGTGCGGGAGTACCTGTCCGAGACCTATGGGAACAAGTTT

crRNA hTFEB.B PAM

c

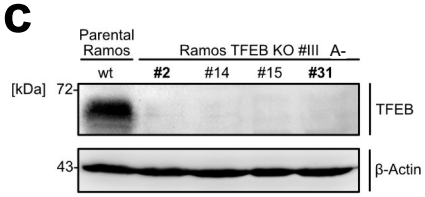

Total screened clones: 39
TFEB-deficient according to blot: 7
⇒ Efficiency: 17.9%

d

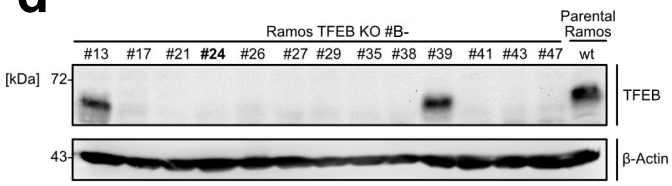

Total screened clones: 48
TFEB-deficient according to blot: 12
⇒ Efficiency: 25.0%

e

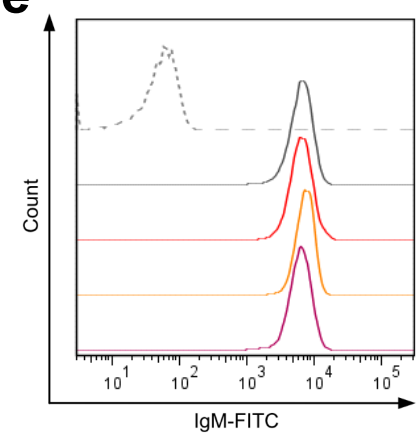

f

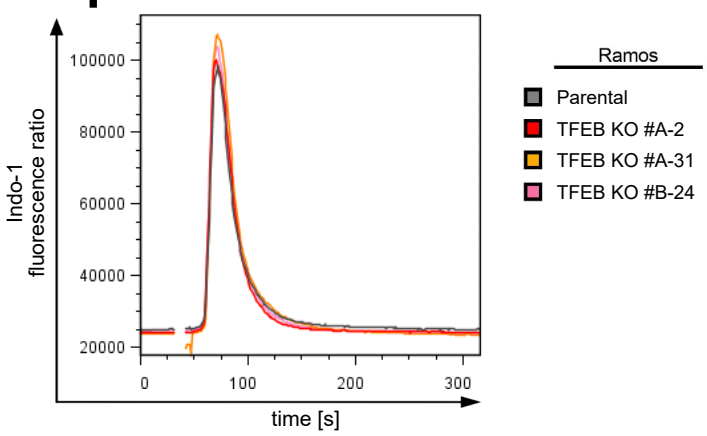

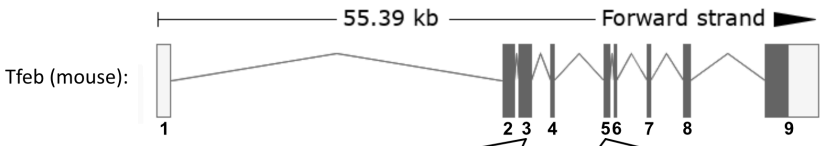

g

GCGGGCTGGACACGTACTGTCCACCTCGGCCGGCAACAGTGCTC

crRNA mTfeb.A PAM

h

CTAGCAGCCACCTGAACGTGTACAGCGGTGACCCCAGGTCAC

crRNA mTfeb.B PAM

i

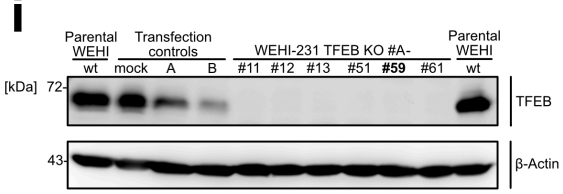

Total screened clones: 47
TFEB-deficient according to blot: 6
⇒ Efficiency: 12.8%

j

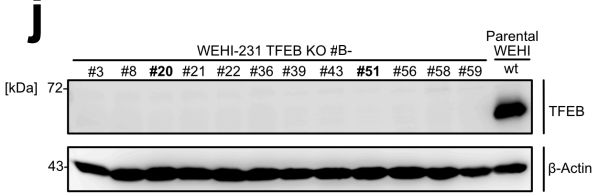

Total screened clones: 52
TFEB-deficient according to blot: 12
⇒ Efficiency: 23.1%

k

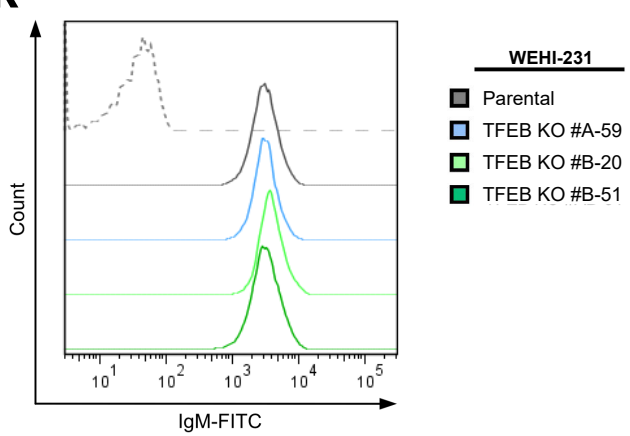

Ext. Data Fig. 5

Extended Data Fig. 5 | Generation of TFEB-deficient B cell clones by CRISPR/Cas9-mediated genome editing. (a-f) Targeted gene disruption in and functional analyses of human Ramos B cells. **(a-b)** Schematic representation of the human TFEB gene locus indicating the targeted exons and including PAM sequence. The gRNA utilized for nucleofection is depicted on the left, the crRNA designed for electroporation is shown on the right. **(c-d)** Immunoblot verification of candidate mutant clones using anti-TFEB antibodies. Relative molecular masses of marker proteins are indicated on the left in kDa and anti-β-Actin staining was used to confirm equal protein loading. **(c)** Clones generated via nucleofection. **(d)** Clones created via the direct electroporation method. Clones used in the study hereafter are marked in bold. **(e)** BCR surface expression of selected TFEB-deficient clones was monitored by flow cytometry using anti-IgM antibodies. **(f)** Selected clones were examined for their BCR-induced Ca^{2+} mobilization capability by flow cytometry using the ratiometric Ca^{2+} indicator Indo-1 AM. After recording of basal Ca^{2+} levels for 30 s, Ramos B cells were BCR-stimulated with 10 µg/ml anti-IgM $F(ab')_2$ fragments and Ca^{2+} influx was monitored for a total of 300 s. **(g-k)** Targeted gene disruption in and functional analyses of murine WEHI-231 B cells. **(g-h)** Schematic representation of the murine *Tfeb* gene locus indicating the targeted exons and sequences (including PAM). Both crRNAs designed for electroporation are shown. **(i-j)** Immunoblot verification of the candidate mutant clones after the first round of screening. **(i)** Clones generated via the crRNA 'mTfeb.A'. **(j)** Clones created using the 'mTfeb.B' crRNA. TFEB-deficient clones used in the study hereafter are marked in bold. **(k)** Flow cytometric analysis of BCR surface expression of selected TFEB-deficient clones.

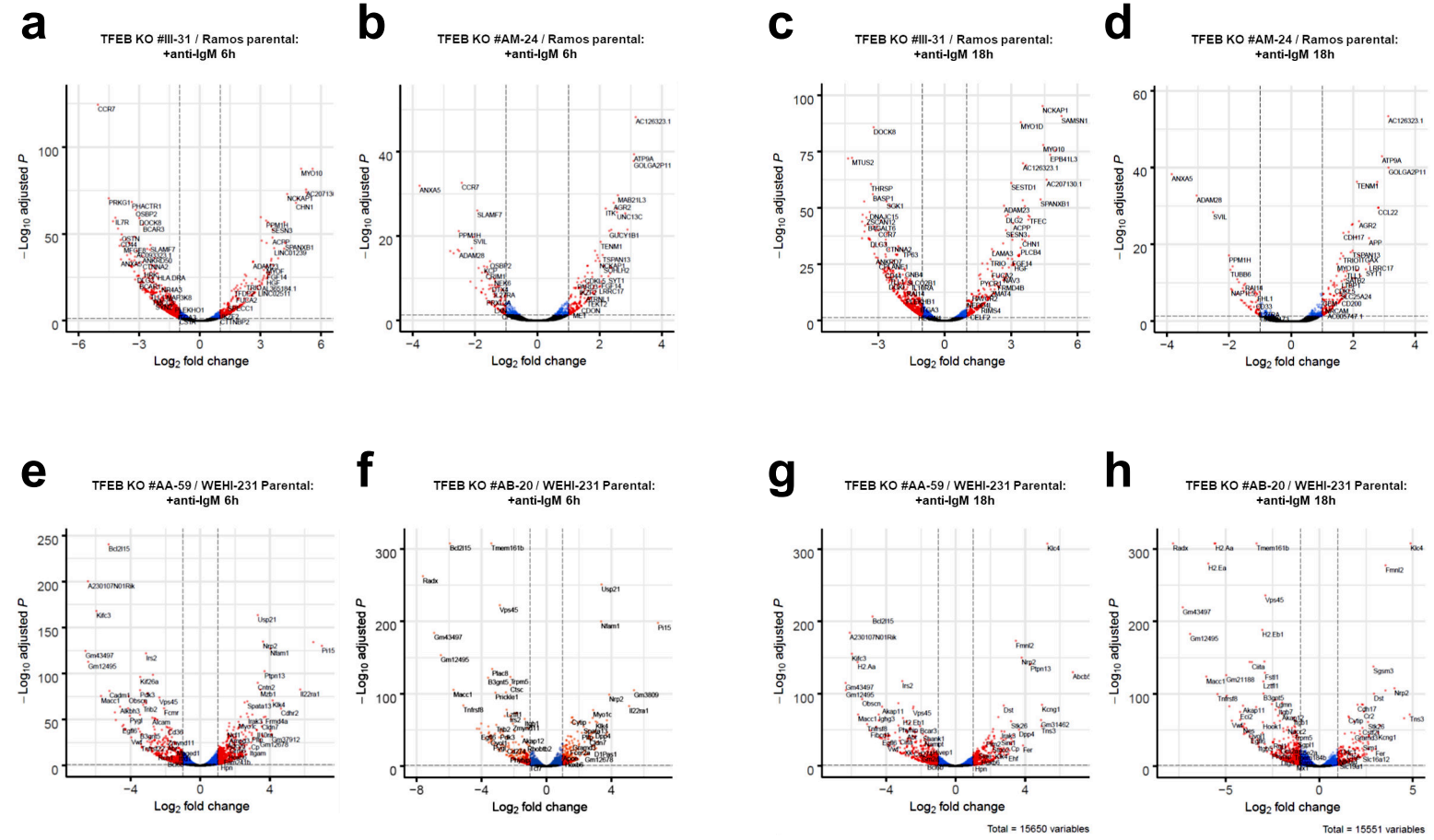

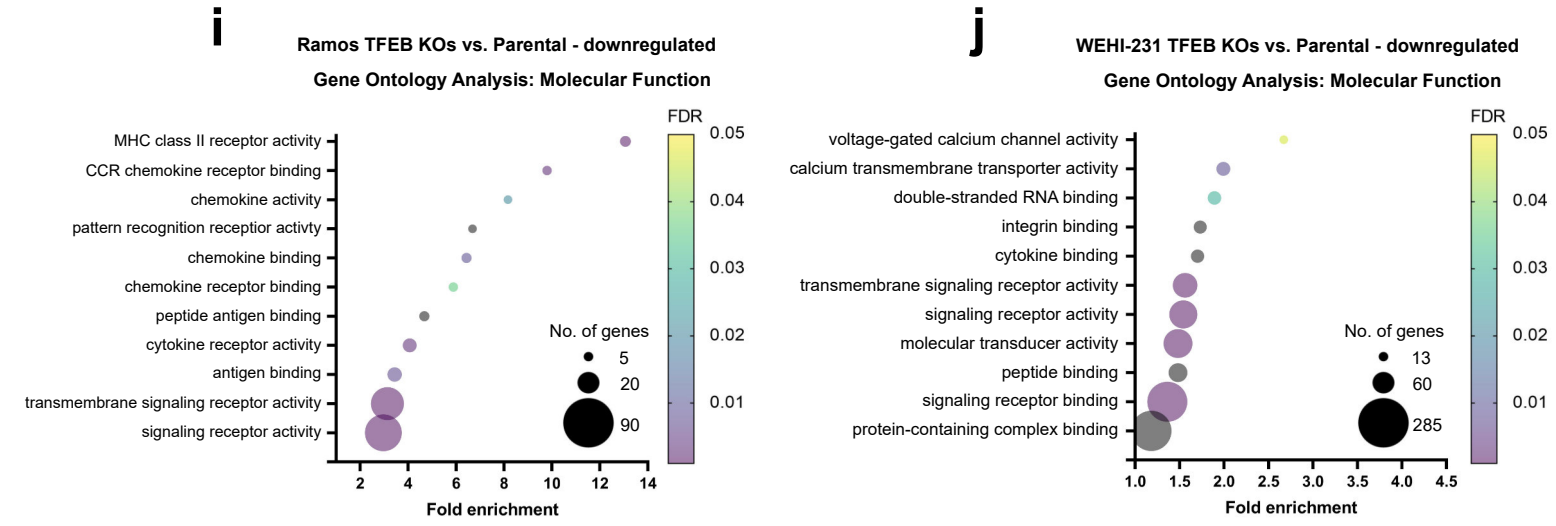

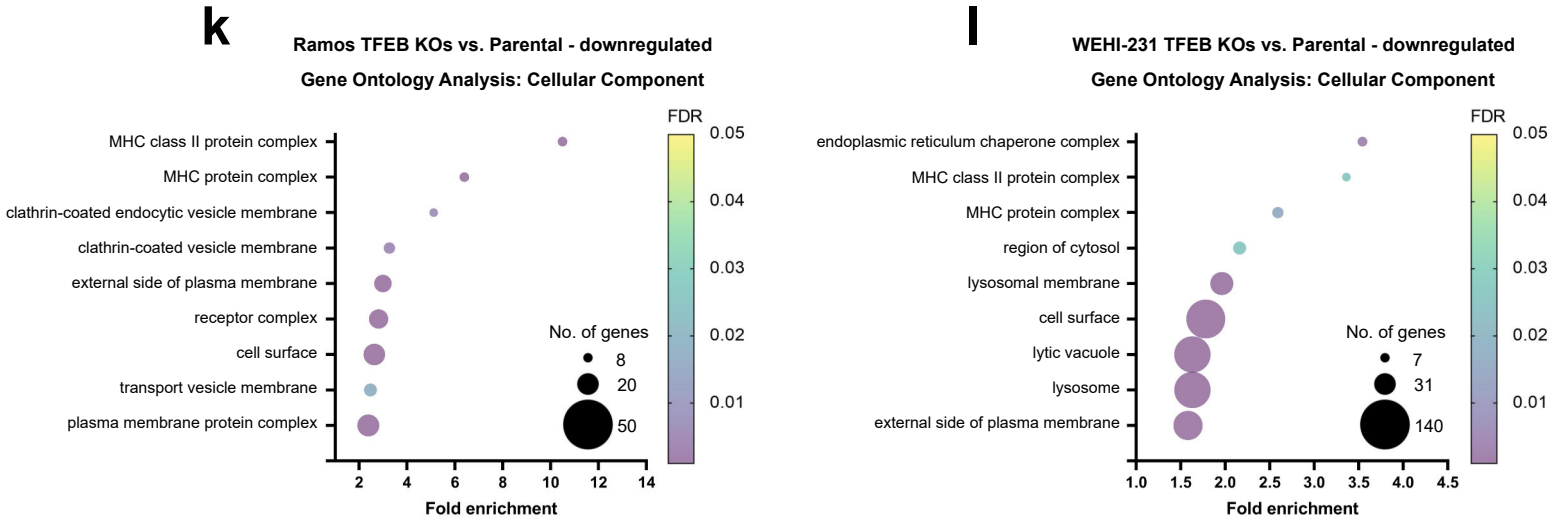

Ext. Data Fig. 6

Extended Data Fig. 6 | RNA seq. analyses and gene ontology mapping of differentially expressed genes in the absence of TFEB. The TFEB-depleted Ramos B cell clones #A-31 and #B-24 as well as the WEHI-231 TFEB knockout clones #A-59 and #B-20 and the respective parental cells were left untreated or BCR-stimulated for 6 h and 18 h. Lysates were subjected to RNA sequencing analysis. **(a-h)** Volcano plots representing differentially expressed genes (DEGs) in TFEB-deficient clones compared to parental cells. Log_2-fold gene expression changes are plotted against the statistical significance presented as log_{10} adjusted p values. Differentially expressed genes (DEGs, red dots) are defined as having a log_2 fold change >1 or <-1 and an adjusted p value of <0.01. **(i-j)** Gene ontology enrichment analysis of the molecular functions of identified downregulated DEGs in TFEB-deficient variants of Ramos **(i)** and WEHI-231 **(j)**. Enrichment of GO terms was assessed via gene ontology analysis using 'GOrilla'. The number of genes assigned to the respective GO term is defined by the bubble size, while the adjusted FDR value is represented through a color gradient. **(k-l)** Cellular components associated with identified downregulated DEGs as defined by gene ontology enrichment analysis in TFEB-deficient variants of Ramos **(k)** and WEHI-231 **(l)**. Enrichment of GO terms was assessed via gene ontology analysis using 'GOrilla'. The number of genes assigned to the respective GO term is defined by the bubble size, while the adjusted FDR value is represented through a color gradient.

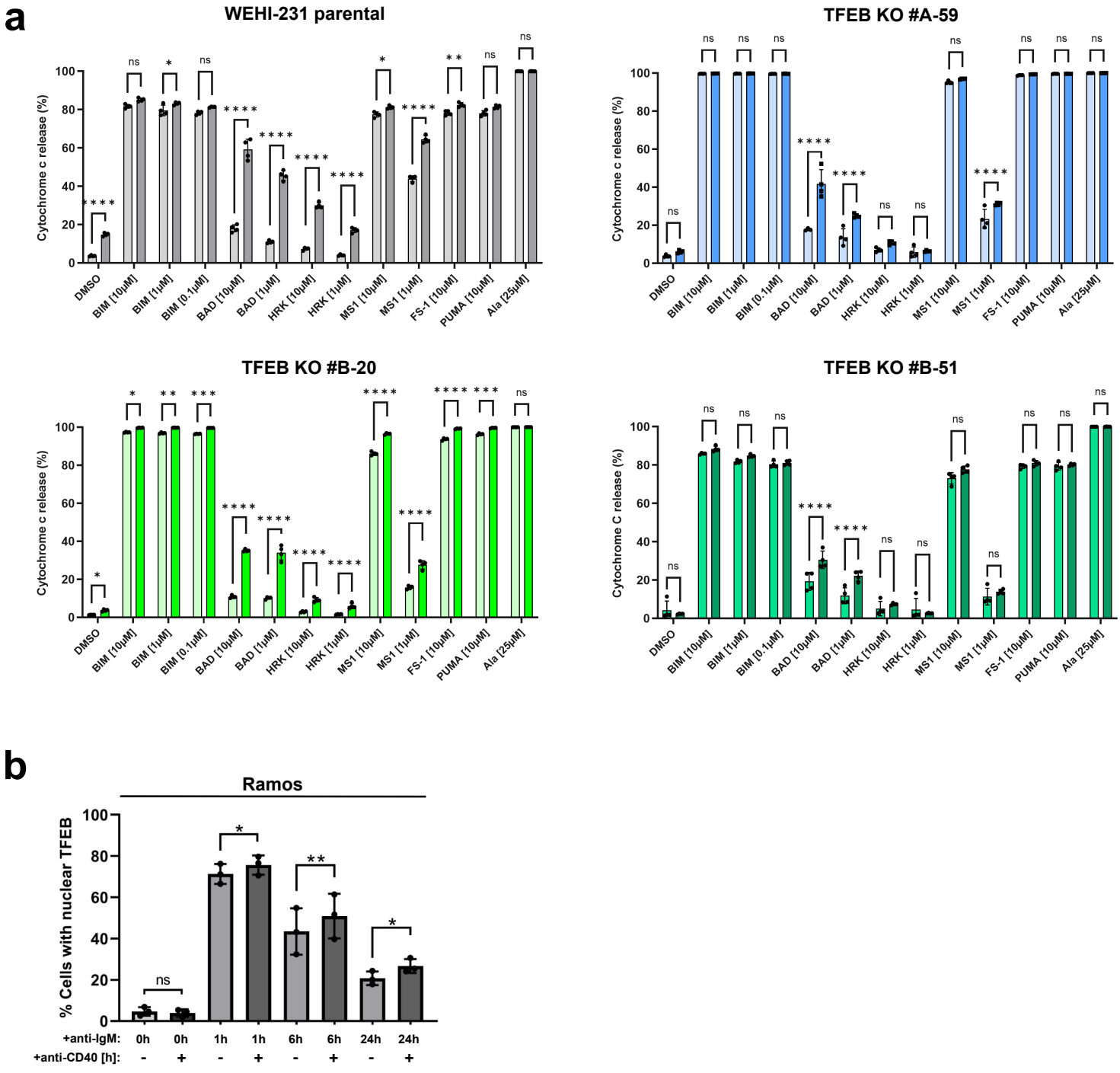

Ext. Data Fig. 7

Extended Data Fig. 7 | Assessment of TFEB-controlled apoptosis and CD40 rescue signals. **(a)** BH3 profiling of wild-type and three independent TFEB-deficient WEHI-231 B cells: Percentage of cytochrome c release upon incubation with the indicated relative molecular concentrations of agonistic BH3 peptides was assessed in resting and in BCR-stimulated cells (6 h). The BCR-induced sensitization for apoptosis is presented as the mean percentage of cytochrome c release of four replicates of unstimulated (light) and stimulated (dark) cells for each cell line. The presented data is representative of three independent experiments. The depicted data shows the mean%±SD of four replicates. Statistical significances were calculated using two-way ANOVA and corrected for multiple testing via Dunnett's method. ****: $p<0.0001$, ***: $p<0.001$, **: $p<0.01$, *: $p<0.05$. **(b)** Wild-type Ramos B cells were left untreated (0) were BCR-stimulated for the indicated time periods in the absence or presence of 10 µg/ml anti-CD40 antibodies. Cells were fixed, permeabilized and the subcellular distribution of TFEB was monitored by imaging flow cytometry using anti-TFEB antibodies and 7-AAD for visualization of the nucleus. Per sample, 10^4 cells were imaged and analyzed. Nuclear translocation of TFEB is depicted as percentage of cells with a similarity score of TFEB/7-AAD ≥1 (bottom). Data is presented as mean±SD of three independent experiments. Statistical significances were calculated using one-way ANOVA and corrected for multiple testing via Tukey's method. **: $p<0.01$, *: $p<0.05$.